Available online at www.sciencedirect.com

SciVerse ScienceDirect

www.elsevier.com/locate/brainres

BRAIN RESEARCH

Research Report

Muscarinic receptor activation disrupts hippocampal sharp wave-ripples

*Hiroaki Norimoto, Mika Mizunuma[1], Daisuke Ishikawa[1], Norio Matsuki, Yuji Ikegaya**

Laboratory of Chemical Pharmacology, Graduate School of Pharmaceutical Sciences, The University of Tokyo, Tokyo 113-0033, Japan

ARTICLE INFO

Article history:
Accepted 19 April 2012
Available online 26 April 2012

Keywords:
Hippocampus
Sharp wave
Ripple
Muscarinic receptor
Calcium imaging
Acetylcholine

ABSTRACT

Cholinergic muscarinic innervations to the hippocampus play a role in learning and memory. Here we report that pharmacological activation of muscarinic receptors eliminates sharp wave-ripple events in the mouse hippocampal CA1 region in vivo and in vitro. This effect was associated with a decorrelation of excitatory synaptic inputs and a net increase in inhibitory conductances in pyramidal neurons. Multineuron calcium imaging revealed that muscarinic activation altered the spatiotemporal pattern of network activities. Thus, cholinergic input is likely to contribute to a neuromodulatory switch of hippocampal network states, as proposed in the "two-stage" model of learning processes.

1. Introduction

Field oscillations prevail in neuronal networks. In particular, the hippocampus is known to exhibit diverse patterns of field oscillations, depending on behavioral states. Theta and gamma oscillations predominate during actively awake state and rapid eye movement (REM) sleep and are believed to encode sensory and cognitive information (Bragin et al., 1995; Buzsaki, 2005; Vanderwolf, 1969). On the other hand, higher-frequency (100–300 Hz), transient (100–250 ms) oscillations called ripples usually occur during quiescent awake state and slow-wave sleep (Buzsaki, 1986; Buzsaki et al., 1992). Ripples appear typically together with sharp waves and are thus referred to herein as sharp wave-ripples (SW-Rs). In rodents, SW-Rs maturate during the first two weeks of postnatal age and are believed to mediate memory consolidation by transferring hippocampal information to stable neocortical storages (Girardeau et al., 2009). In this two-stage model where the hippocampus drifts between two network states, theta-dominant and SW-R-dominant states are thought to reflect neural processes that acquire and stabilize memory, respectively (Buzsaki, 1989); however, the molecular mechanisms that control a switch between these hippocampal oscillation patterns are not fully understood. Acetylcholine is a candidate neurotransmitter that modulates these hippocampal states, because cholinergic muscarinic receptors are involved in learning and memory and synaptic plasticity.

We examined the effect of muscarinic receptor activation on SW-R activity and found that muscarinic agonists suppress SW-Rs in awake mice. We confirmed the same effect in a more simplified, in vitro experiment system. In this in vitro model, we further scrutinized muscarinic-induced suppression of SW-Rs using whole-cell patch-clamp recording and functional multineuron calcium imaging (fMCI). fMCI is a large-scale optical recording technique that determines the timings of action potentials *en masse* from large neuron

* *Corresponding author*. Fax: +81 3 5841 4786.
E-mail address: ikegaya@mol.f.u-tokyo.ac.jp (Y. Ikegaya).
[1] These authors contributed equally to this work.

0006-8993/$ – see front matter © 2012 Elsevier B.V. All rights reserved.
doi:10.1016/j.brainres.2012.04.037

populations, by taking advantage of the fact that an action potential of a neuron reliably evokes a transient increase in the calcium concentration of its cell body (Ikegaya et al., 2004; Sasaki et al., 2007; Takahashi et al., 2007). Compared to conventional electrophysiological recordings, fMCI has unique advantages, including i) simultaneous recording from more than 100 neurons in a wide area, ii) single-cell resolution, iii) identifiable location of neurons, and iv) detection of non-active neurons during the observation period (Namiki and Ikegaya, 2009; Namiki et al., 2009; Takahashi et al., 2010). Using fMCI, we investigated the spatiotemporal patterns in SW-R-relevant spiking of CA1 neurons.

2. Results

2.1. *Muscarinic activation reduces SW-Rs*

Hippocampal LFPs were recorded from the CA1 stratum pyramidale in a total of 15 head-fixed awake mice (Fig. 1A). Spontaneous SW-Rs were evident in all animals tested; the mean event frequency was 0.89±0.28 per second (mean±SD of 15 animals). Within 15 min after intraperitoneal application of 10 mg/kg pilocarpine, a muscarinic receptor agonist, the frequency of SW-Rs decreased to 0.16±0.06 per second (Fig. 1B;

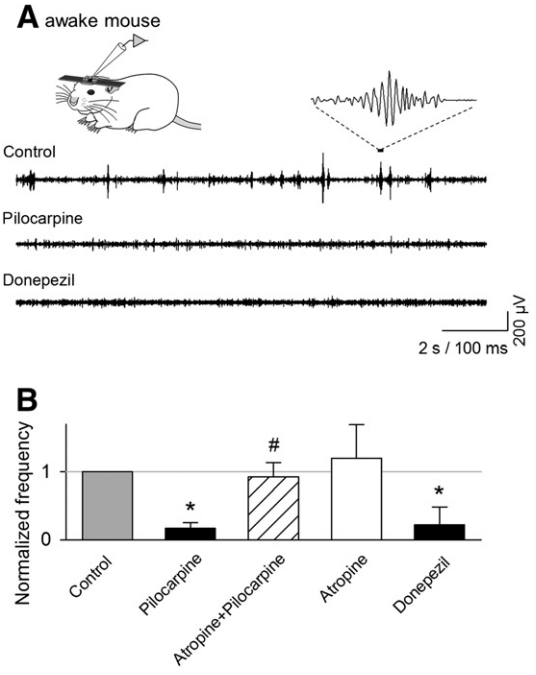

Fig. 1 – Muscarinic activation reduces SW-Rs in vivo. (A) Representative 100–300 Hz filtered traces of LFP recorded from CA1 stratum pyramidale in vivo 3 min before (control, top), 20 min after intraperitoneal treatment with 10 mg/kg pilocarpine (middle), and 30 min after treatment with 3 mg/kg donepezil (bottom). (B) Frequency of SW-R events in mice administered with 10 mg/kg pilocarpine, 50 mg/kg atropine, and 3 mg/kg donepezil (normalized to the pre-treatment control level). *$p<0.05$ versus control, paired *t*-test; #$p<0.05$ *versus* Pilocarpine, Bonferroni/Dun test after one-way ANOVA, $n=5$ mice each.

mean±SD of 5 animals; $p=0.0007$, $t_4=9.48$, paired *t*-test). The effect persisted for at least 1 h. Pilocarpine-induced SW-R suppression did not occur in mice that had received intraperitoneal injection of 50 mg/kg atropine, a muscarinic receptor antagonist, 15 min prior to pilocarpine treatment (Fig. 1B; $p=0.007$ versus pilocarpine alone, $F_{2,12}=11.0$, Bonferroni/Dunn test after one-way ANOVA, $n=5$ mice), while atropine alone did not affect the SW-R frequency (Fig. 1B; $p=0.45$, $t_4=0.85$, paired *t*-test). To estimate whether this effect of muscarinic activation is mediated by either the peripheral or central nervous system, we applied donepezil, an acetylcholine esterase inhibitor that is known to act mainly on the central cholinergic system. Like pilocarpine, donepezil reduced the event frequency of SW-Rs (Fig. 1B; $p=0.003$, $t_4=6.65$, paired *t*-test).

Next, LFPs were recorded from the CA1 stratum pyramidale of obliquely horizontal hippocampal slices (Fig. 2A). As previously reported (Hajos et al., 2009; Maier et al., 2009), SW-Rs emerged spontaneously after an incubation period of 1.5 h under the conditions of a high-speed aCSF perfusion (10 ml/min); the mean SW-R frequency was 0.76±0.55 per second (mean±SD of 88 slices) and did not differ from that in the in vivo hippocampus ($p=0.28$, $t_{96}=0.56$; Student's *t*-test). SW-Rs were suppressed by bath application of pilocarpine, and this effect was dose-dependent in a range between 0.1 and 10 μM (Fig. 2B; $p=0.072$, $t_5=1.82$ for 0.1 μM; $p=4.7\times10^{-7}$, $t_5=20.2$ for 1 μM; $p=3.4\times10^{-10}$, $t_5=68.1$ for 10 μM; paired *t*-test). Similar suppressive effects were produced by bath application of carbachol, a dual agonist of muscarinic and nicotinic receptors, at concentrations ranging from 0.01 to 10 μM (Fig. 2B; $p=0.15$, $t_5=1.13$ for 0.01 μM; $p=0.20$, $t_5=0.93$ for 0.1 μM; $p=1.7\times10^{-3}$, $t_5=5.20$ for 1 μM; $p=3.4\times10^{-10}$, $t_5=68.1$ for 10 μM; paired *t*-test). The suppression of SW-Rs by 10 μM pilocarpine was not observed in the presence of 10 μM atropine or 1 μM pirenzepine, an antagonist of muscarinic M1 receptors (Fig. 2B, $p=1.7\times10^{-10}$ or 3.8×10^{-10} versus 10 μM pilocarpine alone, $F_{2,15}=144.5$, Bonferroni/Dunn test after one-way ANOVA, $n=6$ slices, respectively), while either antagonist alone did not change the SW-R frequency (Fig. 2B, $p=0.13$ or 0.19, $t_5=1.23$ or 0.98, paired *t*-test, respectively). Therefore, M1 receptors primarily mediate the SW-R suppression. Incidentally, we did not observe theta-rhythm oscillations in pilocarpine-treated or carbachol-treated slices. This is likely to be due to the ages of mice employed here. In general, theta oscillations occur in more mature animals. Indeed we found that pilocarpine induced theta oscillations in hippocampal slices prepared from 6-week-old mice (Fig. 2C), which was confirmed by a power spectrum peak at frequencies of 4–8 Hz in the fast Fourier transform of LFP traces (Fig. 2D). In the following experiments, however, we used only 3-to-4-week-old mice, because fMCI is applicable only to juvenile animals (Takahashi et al., 2007).

2.2. *Muscarinic activation induces an unbalance of excitation and inhibition*

There are much literature on the effects of muscarinic activation on synaptic activity of hippocampal neurons, but no studies have elucidated the effects on intrinsically occurring, SW-R-relevant synaptic activity. To monitor ongoing synaptic inputs before and during pilocarpine-induced SW-R suppression, we recorded sEPSCs and sIPSCs from

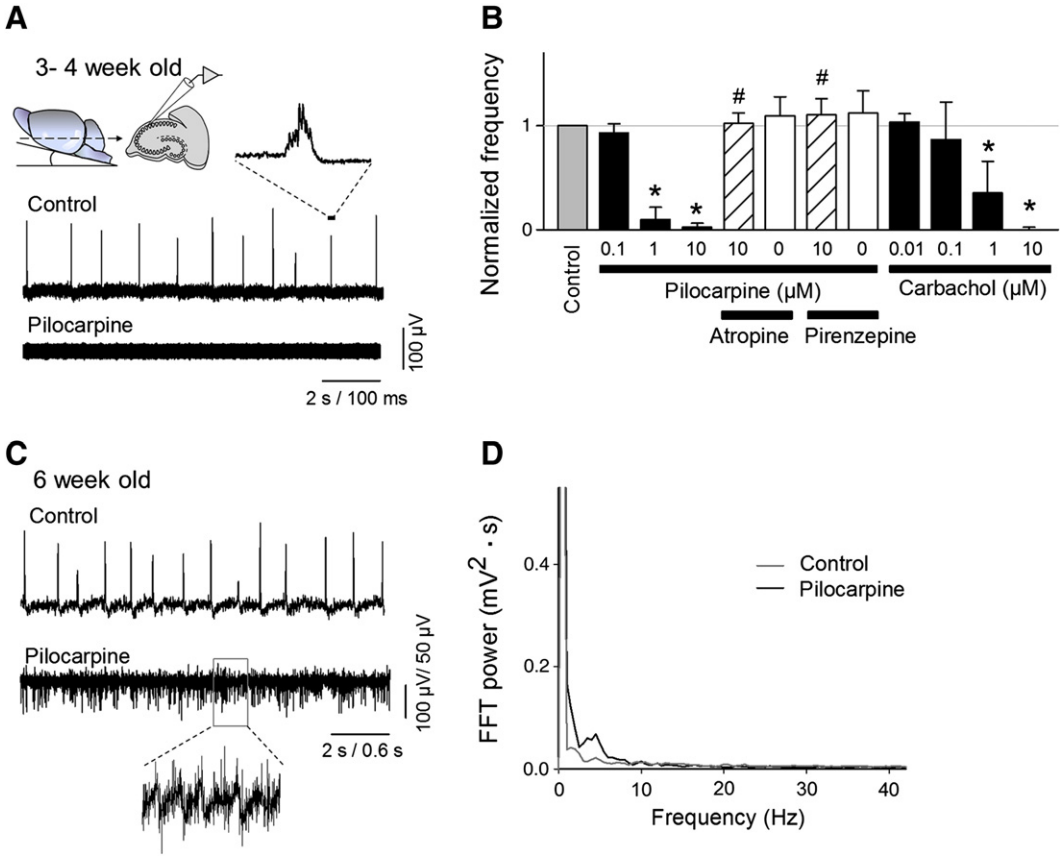

Fig. 2 – Muscarinic activation reduces SW-Rs in vitro. (A) Representative LFPs recorded from CA1 stratum pyramidale in a hippocampal slice prepared from a 3-to-4-week-old mouse 10 min before (control) and 10 min after bath application of 10 μM pilocarpine. (B) SW-R frequency in slices perfused with pilocarpine, carbachol, 10 μM atropine, and 1 μM pirenzepine (normalized to control). $^{*}p<0.05$ versus control, paired t-test, $^{\#}p<0.05$ versus 10 μM pilocarpine, Bonferroni/Dunn test after one-way ANOVA, $n=6$ slices. Error bars indicate SDs. (C) Representative LFPs recorded from CA1 stratum pyramidale in a 6-week-old mouse 10 min before (control) and 10 min after bath application of 10 μM pilocarpine. (D) The fast Fourier transform (FFT) power spectrum of LFPs shown in C (30 s in length). Note pilocarpine induced a spectrum peak at about 5 Hz.

patch-clamped CA1 pyramidal cells. To determine SW-R timings, LFPs were simultaneously recorded from the stratum radiatum close to the apical dendrites of the recorded neurons. sEPSCs and sIPSCs were predominated at clamped voltages of −70 and 0 mV, respectively; spontaneous synaptic inputs recorded at −70 and 0 mV were abolished by bath application of 50 μM D-2-amino-5-phosphonovalerate (AP5) and 10 μM 6-cyano-7-nitroquinoxaline-2,3-dione (CNQX), ionotropic glutamate receptor antagonists (Fig. 3A), and bath application of 100 μM picrotoxin, a $GABA_A$ receptor antagonist (Fig. 3B), respectively.

Under control conditions, large sEPSCs and sIPSCs often occurred together with SW-Rs, whereas small sEPSCs and large sIPSCs appeared to occur more frequently after bath application of 10 μM pilocarpine (Figs. 3C, H). We sought to quantify the effects of pilocarpine. First, we calculated the mean conductance for a period of 3 min. While pilocarpine did not change the excitatory input level (Fig. 3D; $p=0.16$, $t_4=1.72$, paired t-test, $n=5$ neurons in 5 slices prepared from 3 mice), it did increase the mean level of inhibition (Fig. 3I; $p=0.008$, $t_4=8.99$, paired t-test). Therefore, on average, inhibition was strengthened relative to excitation in the presence of pilocarpine.

We next isolated individual events of sEPSCs and sIPSCs and analyzed their properties. Pilocarpine increased the mean frequency of both sEPSCs (Fig. 3E; $p=0.041$, $t_4=2.97$, paired t-test) and sIPSCs (Fig. 3J; $p=0.042$, $t_4=2.96$, paired t-test). Pilocarpine reduced the mean amplitude of sEPSCs (Fig. 3F; $p=0.014$, $t_4=4.15$, paired t-test), but not IPSCs (Fig. 3K; $p=0.74$, $t_4=0.35$, paired t-test). As shown in Fig. 3C, pilocarpine seemed to selectively eliminate large sEPSCs and switch to produce small sEPSCs only. Consistent with this impression, pilocarpine reduced the SD of sEPSC sizes (Fig. 3G; $p=0.036$, $t_4=3.11$, paired t-test). No significant effect was observed for the SD of sIPSC sizes (Fig. 3L; $p=0.15$, $t_4=1.78$, paired t-test). These results indicate that muscarinic activation shifted the balance of excitation and inhibition toward inhibition by increasing the frequency of inhibitory barrages and by reducing largely synchronized excitatory inputs.

2.3. *Optical imaging of SW-Rs*

To examine the spatiotemporal dynamics of neuronal activity during SW-Rs, we used an fMCI technique (Fig. 4A), which probes spikes emitted by individual neurons, based on action

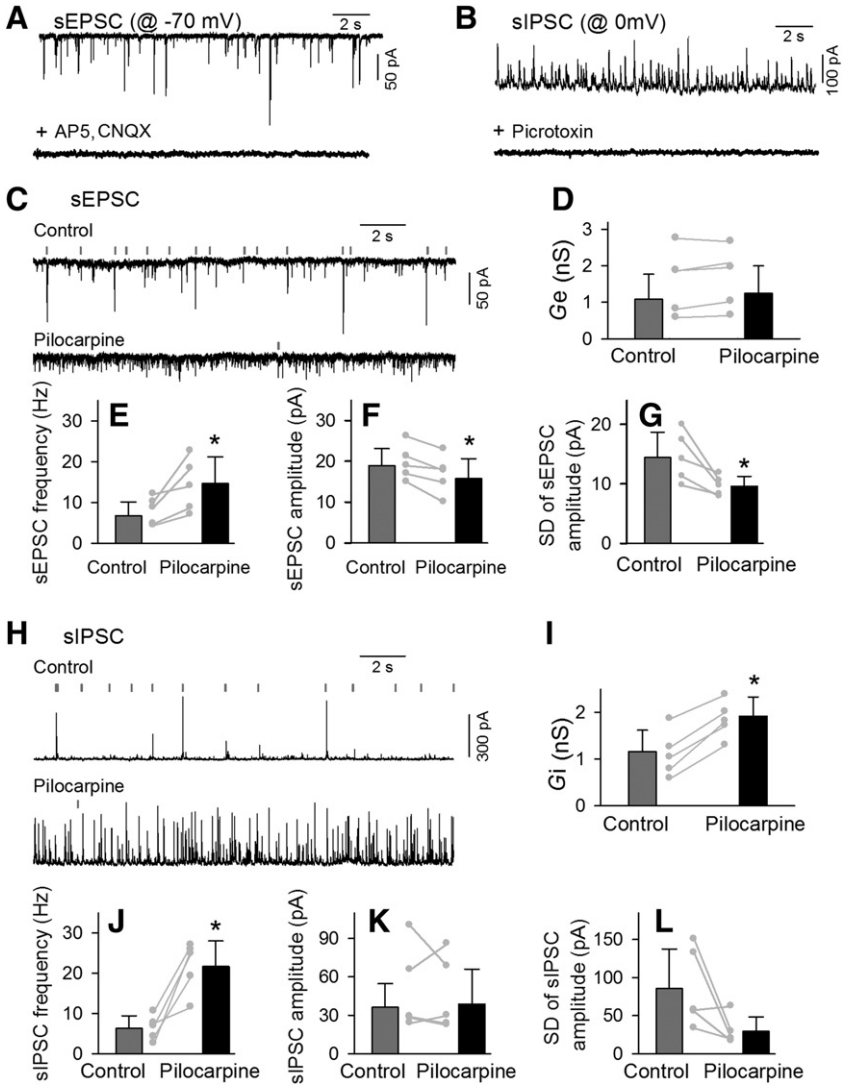

Fig. 3 – Muscarinic activation decorrelates excitatory inputs and increases mass inhibitory conductance. (A) Representative whole-cell traces of sEPSCs (clamped at −70 mV) in a CA1 pyramidal cell in vitro 5 min before (control) and 10 min after bath co-application of 50 μM AP5 and 10 μM CNQX. Similar results were obtained in all 7 slices tested. (B) Representative whole-cell traces of sIPSCs (clamped at −70 mV) in a CA1 pyramidal cell in vitro 5 min before (control) and 10 min after bath application of 100 μM picrotoxin. Similar results were obtained in all 7 slices tested. (C) Representative whole-cell traces of sEPSCs (clamped at −70 mV) in a CA1 pyramidal cell in vitro 5 min before (control) and 10 min after bath application of 10 μM pilocarpine. Vertical lines above each trace indicate the timings of SW-Rs detected in LFPs recorded simultaneously from the CA1 stratum radiatum. (D) Individual data and their means ± SDs of bulk conductance (average of 5 min) of excitatory inputs before (control) and 10 min after bath application of 10 μM pilocarpine. (E–G) Mean frequency of sEPSC events (E), mean amplitude of sEPSC events (F), and SD of individual sEPSC amplitudes (G). (H) Representative whole-cell traces of sIPSCs (clamped at 0 mV) 3 min before (control) and 10 min after pilocarpine application. (I) Bulk conductance (average of 5 min) of inhibitory inputs before (control) and during pilocarpine application. (J–L) Mean sIPSC frequency (J), mean sIPSC amplitude (K), and SD of sIPSC amplitude (L). Error bars indicate SDs of 5 neurons. *$p < 0.05$ versus control, paired t-test.

potential-evoked transient calcium elevations in their cell bodies (Fig. 4B). The calcium transients were monitored at 50 frames per second from an area of approximately $400 \times 250\ \mu m^2$, which contained an average of 43 ± 49 neurons (mean ± SD of 13 slices from 13 mice; ranging from 16 to 203 neurons). LFPs were simultaneously recorded from the same microscopic field (Fig. 4A). A representative raster plot is shown in Fig. 4C, indicating that the activity frequency varied from neuron to neuron and that some of the activities were time-locked to SW-R events. For the entire datasets of 13 slices, 18.8 ± 9.9% of the total calcium activities (mean ± SD) occurred from −50 ms to 50 ms after the peak timings of sharp waves. The mean activity rates reached the maximum at the peak timings of sharp waves (Fig. 4D). On the other hand, activities during individual SW-R events per se were rather sparse, consistent with previous reports (Sun et al., 2012;

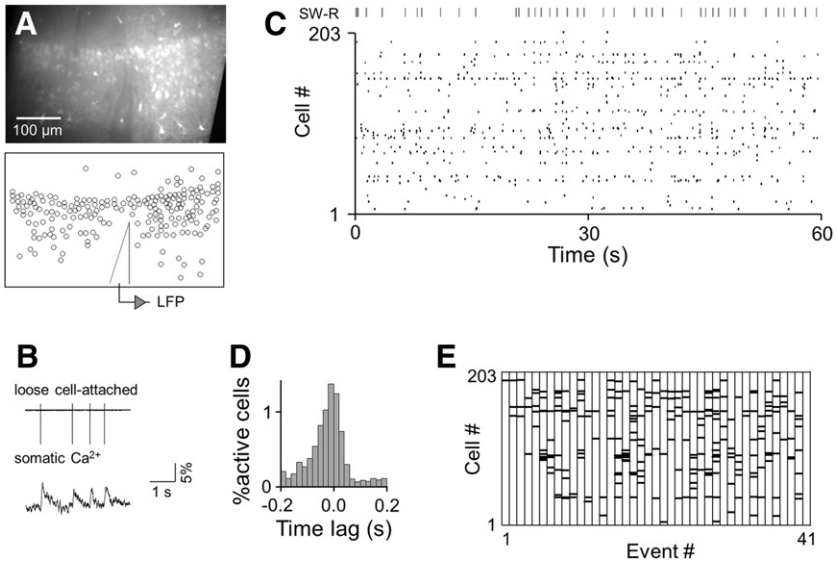

Fig. 4 – Optical imaging of SW-R activity in vitro. (A) A confocal image of the CA1 stratum pyramidale in an OGB-1-loaded slice (top) and the corresponding location map of 203 neurons (bottom). Scale bar: 50 μm. (B) Simultaneous loose cell-attached recording of spikes (top) and calcium imaging from the cell body (bottom) revealed that individual calcium transients reflected spikes. (C) A raster plot of calcium transients in the movie shown in (A). Gray lines above the raster plot indicate the timings of SW-R detected in LFPs recorded simultaneously from the CA1 stratum pyramidale close to the imaged region. (D) A peri-SW-R time histogram of calcium transients. (E) Sets of neurons activated during 41 SW-R events, indicating the diversity of SW-R repertoires.

Ylinen et al., 1995); on average, only 3.0±2.4% of the neurons were activated during a single SW-R event (mean±SD of 4022 SW-R events), whereas 56.6±13.4% neurons participated in at least one SW-R during our observation period of 10 min (mean±SD of 537 neurons). For the dataset shown in Fig. 4C, we plotted an activity map that represents cells participating in each SW-R event (Fig. 4E). This activity plot indicates that different sets of neurons were engaged in different SW-R events, suggesting the diversity of SW-R repertoires.

2.4. *Muscarinic activation alters network activity patterns*

As shown in a raster plot during a 10-min period 5–15 min before and 5–15 min after application of 10 μM pilocarpine (Fig. 5A), the spatiotemporal activity pattern changed in response to muscarinic receptor activation. We pooled data of all 356 neurons from 12 slices and calculated the mean±SD of the total number of activity of individual neurons during a period of 10 min each before and during pilocarpine application (Fig. 5B). Pilocarpine significantly reduced the SD values ($p=2.1\times10^{-41}$, $F_{355,355}=4.43$, F-test), but it did not affect the mean value ($p=0.80$, $t_{507.6}=0.25$, Welch's t-test; $p=0.78$, $t_{355}=0.27$, paired t-test). To further confirm this effect, we re-plotted the normalized activity frequency of individual neurons for each slice (Fig. 5C, $n=12$ slices). Pilocarpine did not change the mean activity frequency (Fig. 5C left; $p=0.10$, $t_{11}=1.34$, paired t-test), but it reduced the SD of the activity frequency per neuron (Fig. 5C right; $p=0.03$, $t_{11}=2.11$, paired t-test). All these analyses suggest that activity that occurred in a relatively few neurons under control conditions became uniform in a larger neuron population after pilocarpine challenge. This notion was confirmed by the cumulative distribution of the activity frequency before and during pilocarpine application (Fig. 5D, $n=334$ neurons).

The activity frequency of individual neurons did not correlate between control and pilocarpine-treated states (Fig. 5E, $R^2=0.02$, $n=334$ neurons), suggesting that different subsets of neurons were recruited after pilocarpine application. To further confirm this, we introduced a 'pairwise synchrony' index to measure synchronization between a given neuron pair, neuron_i and neuron_j. This index was defined as $N_{i,j}/(N_i+N_j-N_{i,j})$, where N_i and N_j represent the number of activities emitted by neuron_i and neuron_j, respectively, during an observation period of 10 min; $N_{i,j}$ represents the number of activities that simultaneously occurred in both neurons within a jitter of 100 ms. The pairwise synchrony index did not correlate between control and pilocarpine-treated states (Fig. 5F, $R^2=0.005$, $n=10{,}067$ pairs). Thus, cohorts of synchronous neurons differed between control and pilocarpine-treated networks, suggesting that muscarinic activation reorganized the cliqueness of spiking activity underlying cell assembly dynamics.

3. Discussion

Although cholinergic modulation of SW-Rs was implied by an in vivo study (Buzsaki et al., 1983), there has been no report directly studying the effect of cholinergic activation on SW-Rs. We found that muscarinic activation disrupts spontaneously occurring SW-Rs in both in vivo and in vitro hippocampal preparations. The results are consistent with previous reports

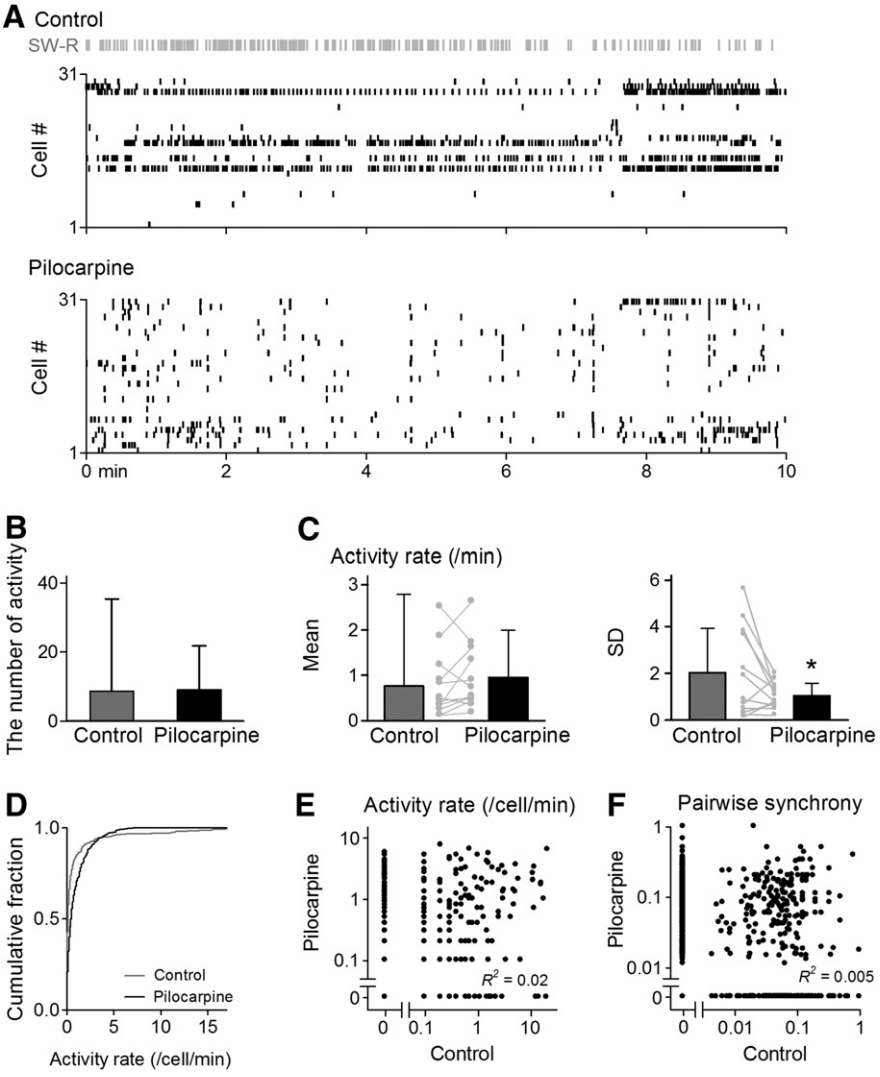

Fig. 5 – Muscarinic activation alters network activity patterns. (A) Raster plots of calcium transient before (top) and during bath application of 10 μM pilocarpine (bottom). Gray lines above each raster plot indicate the SW-R timings. (B) Mean ± SD of the number of calcium activities of 334 individual neurons obtained from 12 slices for a period of 10 min each before and during pilocarpine application. (C) Mean (left) and SD (right) of the mean activity frequency of individual neurons within slices before and during pilocarpine application. Error bars indicate SDs of 12 slices. *$p < 0.05$, paired t-test. (D) Cumulative distribution of the activity frequency of the total 334 neurons in 12 slices before and during pilocarpine application. (E) Relationship of the activity frequency of individual neurons between control (ordinate) and pilocarpine-treated slices (abscissa). Each dot indicates a single neuron. $n = 334$ neurons. (F) Functional correlations in the activity patterns between given neuron pairs. Each dot indicates a single neuron pair. $n = 10{,}067$ pairs.

showing that the level of acetylcholine release elevates during active awake state and REM sleep and declines during quiescent awake state and slow-wave sleep and also that cholinergic activation induces REM sleep (Benington and Heller, 1995).

We conducted intracellular recordings of subthreshold synaptic inputs to elucidate the network mechanisms underlying muscarinic suppression of SW-Rs. After pilocarpine perfusion, large sEPSCs time-locked to SW-Rs disappeared, and small sEPSCs became dominant. Nonetheless, the net level of excitation did not change, because it was compensated by an increased sEPSC frequency. Consistent with this finding, our fMCI data revealed that pilocarpine treatment did not alter the overall level of neuronal activities, even though it substantially reorganized the spatiotemporal patterns of network activity. Moreover, the fMCI data showing that activities in pilocarpine-treated slices were widespread in larger neuron populations is also in accordance with an increase in small sEPSCs, i.e., decorrelation of excitatory neurons. On the other hand, the net conductance of inhibition increased in pilocarpine-treated slices. This was due to an increase in the sIPSC frequency, but not to a change in the sIPSC size. This implies that muscarinic activation increased the frequency in synchronous events of GABAergic

interneurons. The resultant excitatory-versus-inhibitory unbalance may contribute to a spike decorrelation among excitatory neurons and thereby cause SW-R suppression. Because muscarinic M1 receptors are expressed in GABAergic interneurons in the hippocampus (Lawrence et al., 2006; Shen et al., 2009), they may modulate inhibitory network activity.

Our results suggest that muscarinic neuromodulation could contribute to a molecular switch between theta and SW-R states. Given that sets of active neurons were substantially different between these two states, different network principles may operate to generate these two states, as being suggested by the two-stage model (Buzsaki, 1989) as well as computation simulation based on behavioral and pharmacological evidence (Hasselmo et al., 2000). Cholinergic input to the hippocampus arises primarily from the medial septal area and diagonal band of Broca, although intrinsic cholinergic interneurons are also described within the hippocampus (Frotscher and Leranth, 1985). These cholinergic sources may play a role in switching between theta and SW-R oscillations.

4. Conclusion

We examined the effect of muscarinic receptor activation on SW-R activity, which spontaneously occurs in the hippocampus of awake mice and oblique brain slices. Muscarinic receptor activation agonists were found to suppress SW-Rs in both in vivo and in vitro preparations, an effect that was blocked by muscarinic M1 receptor antagonists. Electrophysiological and optophysiological analyses revealed that muscarinic receptor activation caused a state transition of ongoing network activity. These results are consistent with the "two-stage" hypothesis of memory storage and consolidation.

5. Experimental procedures

5.1. *Animal ethics*

Experiments were performed with the approval of the animal experiment ethics committee at The University of Tokyo (approval numbers: A21-6 and 19-35) and according to The University of Tokyo guidelines for the care and use of laboratory animals.

5.2. *Drug*

Carbachol, pilocarpine, atropine sulfate monohydrate, donepezil hydrochloride, pirenzepine dihydrochloride, picrotoxin, AP5, and CNQX were dissolved at 10 mM in water or saline and stocked at 4 °C. Immediately before use, they were diluted to the final concentration with saline or artificial cerebrospinal fluid (aCSF) containing (in mM): 127 NaCl, 3.5 KCl, 1.24 KH_2PO_4, 1.2 $MgSO_4$, 2.0 $CaCl_2$, 26 $NaHCO_3$, and 10 D-glucose.

5.3. *Animal preparation*

Recordings were conducted from awake, head-restricted mice (Minamisawa et al., 2011). Male ICR mice (21–25-day-old, SLC, Shizuoka, Japan) were anesthetized with ketamine (50 mg/kg, i.p.) and xylazine (10 mg/kg, i.p.). The anesthesia was confirmed by a lack of paw withdrawal, whisker movement, and eye blink reflexes. A heating pad maintained the rectal temperature at 37 °C. The skin was removed and the animal was implanted with a metal head-holder. After two days of recovery, the head-fixation training on a custom-made stereotaxic fixture was repeated for 1–3 h per day until the implanted animal learned to remain quiet. This habituation procedure required 6 to 10 days, depending on the animal. During and after each session, the animal was rewarded with free access to sucrose-containing water. During the last 3 sessions, sham experiments were conducted to habituate the animal to experimental conditions and noise. On the final days, the animals were able to be kept virtually immobile, i.e., quiet awake, for more than 2 h. After full habituation, the animal was anesthetized with ketamine/xylazine and analgesized with 0.2% lidocaine during the entire period of experiments. Throughout experiments, a heating pad maintained the rectal temperature at 37 °C. Craniotomy ($1 \times 1\ mm^2$), centered at 2.5 mm posterior and 2.2 mm lateral to the bregma, was performed, and the dura was surgically removed. The exposed cortex surface was covered with 1.7% agar.

5.4. *Slice preparation*

Acute slices were prepared from the hippocampal formation of C57BL/6J mice (Ueno et al., 2002). Briefly, obliquely horizontal slices of the hippocampus (400 μm thick) at an angle of 12.7° in the fronto-occipital direction (Behrens et al., 2005) were prepared using a vibratome in ice-cold oxygenated cutting solution consisting of 222.1 sucrose, 27 $NaHCO_3$, 1.4 NaH_2PO_4, 2.5 KCl, 1 $CaCl_2$, 7 $MgSO_4$, and 0.5 ascorbic acid. Slices were transferred in oxygenated aCSF. Subsequently, slices were allowed to recover for at least 1.5 h in a submerge chamber filled with oxygenated aCSF at room temperature. Experiments were performed in a submerge chamber perfused at 10 ml/min with oxygenated aCSF at 35–37 °C.

5.5. *Electrophysiological recording*

Local field potentials (LFPs) in vivo and in vitro were recorded from CA1 stratum pyramidale or radiatum with borosilicate glass pipettes (1–2 MΩ) filled with aCSF (Kuga et al., 2011; Sun et al., 2012). Whole-cell patch clamp recordings were obtained from CA1 pyramidal cells visually identified under infra-red differential interference contrast microscopic control. Patch pipettes (4–9 MΩ) were filled with cesium-based solution consisting of (mM): 125 Cs-$MgSO_4$, 10 CsCl, 10 HEPES, 10 phosphocreatine, 4 MgATP, 0.4 Na_2GTP, and 2 QX-314. Spontaneous excitatory and inhibitory postsynaptic currents (sEPSCs and sIPSCs) were dominated at clamped voltages of −70 and 0 mV, respectively, without using receptor antagonists (Sasaki et al., 2011; Takahashi et al., 2012). Recordings were amplified by MultiClamp 700B and analyzed by pCLAMP 10 (Molecular Devices, Union City, CA, USA). Signals were digitized at 10,000 Hz and filtered with a band of 1–2000 Hz. Off-line analysis was conducted using custom-made routines developed in a MATLAB environment (MathWorks, Natick, MA, USA). SW-Rs were detected by thresholding filtered traces, based on the signal-to-noise ratio. For SW-R in vivo,

LFP traces were band-pass filtered at 100–300 Hz and thresholded at 5 times above the standard deviation (SD) of baseline noise, whereas for SW-Rs in vitro, LFP traces were band-pass filtered at 2–30 Hz and thresholded at 4 times above the SD of baseline noise. The detected events were all inspected by eye and manually rejected if they were erroneously detected. The ripple events with durations of less than 30 ms were also eliminated, because most of them were recording artifacts.

5.6. *Optical recording*

Functional multineuron calcium imaging (fMCI) was conducted using acute slices loaded locally with Oregon Green BAPTA-1AM (OGB-1) (Takahashi et al., 2011). OGB-1 was dissolved in DMSO containing 10% Pluronic F-127 to yield a concentration of 200 μM. Immediately before use, this solution was 10× diluted with aCSF and loaded into pipettes (3–5 MΩ). The tip of the pipette was inserted into the CA1 stratum pyramidale, and a pressure was applied using a 10-ml syringe pressurizer (50–60 hPa for 3–5 min). Fluorophores were excited at 488 nm with a laser diode (HPU50101PFS, FITEL, Tokyo, Japan) and visualized using a 507-nm long-pass emission filter. Videos were at 50 frames/s using a 16× objective (CFI75LWD16xW, Nikon, Tokyo, Japan), a Nipkow-disk confocal microscope (CSU-X1; Yokogawa Electric, Tokyo, Japan), and a cooled EM-CCD camera (iXon DU897, Andor, Belfast, UK). The fluorescence change was measured as $(F_t - F_0)/F_0$, where the F_t is the fluorescence intensity at a given time point; F_0 is the baseline. Spike-elicited calcium transients were semi-automatically detected with a custom-written program in Visual Basic version 6.0 (Microsoft, Seattle, WA, USA) and then visually inspected (Ikegaya et al., 2004).

Acknowledgments

This work was supported in part by Grants-in-Aid for Science Research (nos. 18021008, 22115003, 22115013, 22650080, and 22680025) from the Ministry of Education, Culture, Sports, Science and Technology of Japan; the Suzuken Memorial Foundation; the Kanae Foundation for the Promotion of Medical Science; the Daiichi-Sankyo Foundation of Life Science; and the Funding Program for Next Generation World-Leading Researchers (no. LS023).

REFERENCES

Behrens, C.J., van den Boom, L.P., de Hoz, L., Friedman, A., Heinemann, U., 2005. Induction of sharp wave-ripple complexes in vitro and reorganization of hippocampal networks. Nat. Neurosci. 8, 1560–1567.

Benington, J.H., Heller, H.C., 1995. Monoaminergic and cholinergic modulation of REM-sleep timing in rats. Brain Res. 681, 141–146.

Bragin, A., Jando, G., Nadasdy, Z., Hetke, J., Wise, K., Buzsaki, G., 1995. Gamma (40–100 Hz) oscillation in the hippocampus of the behaving rat. J. Neurosci. 15, 47–60.

Buzsaki, G., 1986. Hippocampal sharp waves: their origin and significance. Brain Res. 398, 242–252.

Buzsaki, G., 1989. Two-stage model of memory trace formation: a role for "noisy" brain states. Neuroscience 31, 551–570.

Buzsaki, G., 2005. Theta rhythm of navigation: link between path integration and landmark navigation, episodic and semantic memory. Hippocampus 15, 827–840.

Buzsaki, G., Leung, L.W., Vanderwolf, C.H., 1983. Cellular bases of hippocampal EEG in the behaving rat. Brain Res. 287, 139–171.

Buzsaki, G., Horvath, Z., Urioste, R., Hetke, J., Wise, K., 1992. High-frequency network oscillation in the hippocampus. Science 256, 1025–1027.

Frotscher, M., Leranth, C., 1985. Cholinergic innervation of the rat hippocampus as revealed by choline acetyltransferase immunocytochemistry: a combined light and electron microscopic study. J. Comp. Neurol. 239, 237–246.

Girardeau, G., Benchenane, K., Wiener, S.I., Buzsaki, G., Zugaro, M.B., 2009. Selective suppression of hippocampal ripples impairs spatial memory. Nat. Neurosci. 12, 1222–1223.

Hajos, N., Ellender, T.J., Zemankovics, R., Mann, E.O., Exley, R., Cragg, S.J., Freund, T.F., Paulsen, O., 2009. Maintaining network activity in submerged hippocampal slices: importance of oxygen supply. Eur. J. Neurosci. 29, 319–327.

Hasselmo, M.E., Fransen, E., Dickson, C., Alonso, A.A., 2000. Computational modeling of entorhinal cortex. Ann. N. Y. Acad. Sci. 911, 418–446.

Ikegaya, Y., Aaron, G., Cossart, R., Aronov, D., Lampl, I., Ferster, D., Yuste, R., 2004. Synfire chains and cortical songs: temporal modules of cortical activity. Science 304, 559–564.

Kuga, N., Sasaki, T., Takahara, Y., Matsuki, N., Ikegaya, Y., 2011. Large-scale calcium waves traveling through astrocytic networks in vivo. J. Neurosci. 31, 2607–2614.

Lawrence, J.J., Statland, J.M., Grinspan, Z.M., McBain, C.J., 2006. Cell type-specific dependence of muscarinic signalling in mouse hippocampal stratum oriens interneurones. J. Physiol. 570, 595–610.

Maier, N., Morris, G., Johenning, F.W., Schmitz, D., 2009. An approach for reliably investigating hippocampal sharp wave-ripples in vitro. PLoS One 4, e6925.

Minamisawa, G., Funayama, K., Matsuki, N., Ikegaya, Y., 2011. Intact internal dynamics of the neocortex in acutely paralyzed mice. J. Physiol. Sci. 61, 343–348.

Namiki, S., Ikegaya, Y., 2009. Current application and technology of functional multineuron calcium imaging. Biol. Pharm. Bull. 32, 1–9.

Namiki, S., Matsuki, N., Ikegaya, Y., 2009. Large-scale imaging of brain network activity from >10,000 neocortical cells. Nat Precedings (2009.2893, 1).

Sasaki, T., Matsuki, N., Ikegaya, Y., 2007. Metastability of active CA3 networks. J. Neurosci. 27, 517–528.

Sasaki, T., Matsuki, N., Ikegaya, Y., 2011. Action-potential modulation during axonal conduction. Science 331, 599–601.

Shen, J.X., Tu, B., Yakel, J.L., 2009. Inhibition of alpha 7-containing nicotinic ACh receptors by muscarinic M1 ACh receptors in rat hippocampal CA1 interneurones in slices. J. Physiol. 587, 1033–1042.

Sun, Y., Norimoto, H., Pu, X.P., Matsuki, N., Ikegaya, Y., 2012. Cannabinoid receptor activation disrupts the internal structure of hippocampal sharp wave-ripple complexes. J. Pharmacol. Sci. 118, 288–294.

Takahashi, N., Sasaki, T., Usami, A., Matsuki, N., Ikegaya, Y., 2007. Watching neuronal circuit dynamics through functional multineuron calcium imaging (fMCI). Neurosci. Res. 58, 219–225.

Takahashi, N., Takahara, Y., Ishikawa, D., Matsuki, N., Ikegaya, Y., 2010. Functional multineuron calcium imaging for systems pharmacology. Anal. Bioanal. Chem. 398, 211–218.

Takahashi, N., Oba, S., Yukinawa, N., Ujita, S., Mizunuma, M., Matsuki, N., Ishii, S., Ikegaya, Y., 2011. High-speed multineuron calcium imaging using Nipkow-type confocal microscopy. Curr. Protoc. Neurosci. 2, 14.

Takahashi, N., Kitamura, K., Matsuo, N., Mayford, M., Kano, M., Matsuki, N., Ikegaya, Y., 2012. Locally synchronized synaptic inputs. Science 335, 353–356.

Ueno, S., Tsukamoto, M., Hirano, T., Kikuchi, K., Yamada, M.K., Nishiyama, N., Nagano, T., Matsuki, N., Ikegaya, Y., 2002. Mossy fiber Zn^{2+} spillover modulates heterosynaptic N-methyl-D-aspartate receptor activity in hippocampal CA3 circuits. J. Cell. Biol. 158, 215–220.

Vanderwolf, C.H., 1969. Hippocampal electrical activity and voluntary movement in the rat. Electroencephalogr. Clin. Neurophysiol. 26, 407–418.

Ylinen, A., Bragin, A., Nadasdy, Z., Jando, G., Szabo, I., Sik, A., Buzsaki, G., 1995. Sharp wave-associated high-frequency oscillation (200 Hz) in the intact hippocampus: network and intracellular mechanisms. J. Neurosci. 15, 30–46.